Available online at www.sciencedirect.com
ScienceDirect
Solar Energy Materials & Solar Cells 92 (2008) 799–804
Solar Energy Materials and Solar Cells
www.elsevier.com/locate/solmat

Photo-degradation and stabilization effects in operating organic photovoltaic devices by joint photo-current and morphological monitoring

B. Paci[a,*], A. Generosi[a], V. Rossi Albertini[a], P. Perfetti[a], R. de Bettignies[b], C. Sentein[c]

[a]*ISM-C.N.R., Area di Ricerca di Tor Vergata, Via del Fosso del Cavaliere 100, 00133 Roma, Italy*
[b]*Laboratoire Composants Solaires, CEA INES-RDI, Savoie Technolac, BP 332, 50 avenue du lac Léman, 73377 Le Bourget du Lac, France*
[c]*CEA Saclay, DRT-LITEN-DSEN-GENEC-L2C, F91191 Gif-sur-Yvette, France*

Received 18 October 2007; received in revised form 12 February 2008; accepted 13 February 2008
Available online 8 April 2008

Abstract

We report on a joint morphological/photoelectrical study of polymer-based photovoltaic (PV) cells in working conditions. The bulk heterojunction devices investigated are based on an active layer of poly(3-hexyl thiophene) blended with methano-fullerene, combining good PV performances with promising stability. The set-up adopted allowed the electrical properties of the device to be directly correlated to the modification of the electrode morphological parameters (thickness and roughness), which were obtained by in situ energy dispersive X-ray reflectometry (EDXR). The results of this joint time-dependent characterization demonstrated how the observed photo-induced oxidation process, limited to the buried electrode interface, is responsible for a fast decrease in the photo-current. The time-resolved measurements allowed to rule out the dynamics of the morphological changes and showed that the interface morphology may be stabilized by annealing treatments, with a significant improvement of the cell efficiency.

Keywords: Bulk heterojunction; Organic photovoltaic cells; *In situ* morphological monitoring; Degradation; Stability

1. Introduction

Organic photovoltaic cells, which provide low-cost conversion of solar energy, are among the possible solutions to present day energy problems. Although much less efficient than silicon cells, organic solar cells exhibit a unique combination of interesting properties, including low cost, flexibility and the ability to cover large surfaces. Furthermore, the latest advances in the field of plastic solar cells have brought these devices to a level at which commercialization is a realistic prospect. A considerable advance in the field was obtained in the mid-1990s, when it was demonstrated that ultra-fast electron transfer may be photo-induced from a donor material to fullerene [1]. Nowadays, photo-induced electron transfer from a conjugated polymer (donor) to buckminsterfullerene C_{60} (acceptor) is the basic mechanism utilized in polymer-based photovoltaic cells, providing a molecular approach to high-efficiency photovoltaic conversion. An increasing number of research groups have recently moved towards polythiophene and its derivatives, since devices based on this polymer combine good photovoltaic (PV) performances and promising stability [2–5]. Notable progress has been made in recent years and, using poly(3-hexyl thiophene) (P3HT) blended with methano-fullerene [6,6]-phenyl C_{61}-butyric acid methyl ester (PCBM), efficiencies exceeding 6% [6–10] were obtained.

A more thorough inspection of the various mechanisms involved in the conversion of solar energy is required for a substantial improvement in this technology. The main points which need to be addressed are the stability and lifetime of the cells, which could be investigated by observing the behaviour of devices based on alternative or simplified architectures. New characterization techniques are therefore of extreme importance in order to better

*Corresponding author. Tel.: +39 06 4993 4174; fax: +39 06 4993 4153.
E-mail address: Barbara.Paci@ism.cnr.it (B. Paci).

0927-0248/$ - see front matter © 2008 Elsevier B.V. All rights reserved.
doi:10.1016/j.solmat.2008.02.019

understand the changes of the organic layers upon cell working and their effect on the device's lifetime.

With this goal, the present paper reports the first joint photo-current and time-resolved energy dispersive X-ray reflectometry (EDXR) characterization of this type of cells.

2. Results and discussion

In the present work, the time-resolved EDXR was used to address the morphological stability of the electrode–active layer interface, which is considered to be a critical point for improvement of organic PV devices. The use of the time-resolved EDXR technique enables the changes in thickness and roughness of the layers of stratified systems to be monitored [11–13].

The X-ray reflectometry is commonly utilized to probe the properties of surfaces and interfaces of layered samples, like films deposited on substrates, multilayers, superlattices, etc. This technique is based on the optical properties of X-rays, whose refraction index in a material $n = 1-(\lambda^2/2\pi)\rho r_0 Z^2$ (λ = incident wavelength, ρ = material density, r_0 = classical electron radius and Z = atomic number), although very close to 1, is not exactly unitary. As a consequence, the Snell rule still applies and, at the critical angle, it can be written as [14] $\cos\theta_c = n$. Expanding the right-hand side to the second order: $1-\theta_c^2/2 = 1-\rho\lambda^2 r_0 Z^2/2\pi$, which corresponds to $(\theta_c/\lambda) = Z(\rho r_0/\pi)^{1/2} = \text{constant}$, where $\theta_c/\lambda \approx \sin\theta_c/\lambda \propto q_c$ (critical value of scattering parameter $q_c = 4\pi\sin\theta_c/\lambda$).

Therefore, the variable on which the reflected intensity actually depends is not the deflection angle only but, rather, the scattering parameter $q = 4\pi\sin\theta/\lambda = (2/hc)E\sin\theta$ (E = radiation energy, h = Plank's constant, c = velocity of light), as in the case of the X-ray diffraction. Hence, in analogy with diffraction [14,15], two ways can be utilized to perform the q-scan, namely, either using a monochromatic beam and executing an angular scan (angular dispersive (AD) mode), or using a polychromatic X-ray beam at a fixed angle and carrying out an energy scan (energy dispersive (ED) mode).

Although affected by a lower resolution, the ED [11] technique has some advantages on the laboratory AD counterpart [14] connected to the immobility of the experimental apparatus during data collection. Indeed, in the grazing geometry required for this kind of measurements, even minimal misalignments of the sample may induce relevant relative errors during the angular scan. In particular, if many scans have to be carried out consecutively, as in the present case, reproducibility problems that may arise because of the mechanical movements of the diffractometer arms are prevented by EDXR.

Finally, when laboratory sources (X-ray tubes) are used, the data collection is shorter in ED since the number of photons concentrated in the monochromatic fluorescence lines (used as primary beam in AD) is much lower than the number of photons distributed along the white Bremmstrahlung component (primary beam in ED).

The EDXR measurements were performed using a non-commercial laboratory energy dispersive X-ray reflectometer, fully described elsewhere [11] in the working conditions described in the experimental part.

Recent results on a similar cell, based on MDMO-PPV (poly(2-methoxy-5-(3′,7′-dimethyloctyloxy)-1,4-phenylene-vinylene) blended with PCBM as bulk heterojunction, showed the onset of photo-induced oxidation of the Al electrode at the buried interface [12]. A cell with a different structure is utilized in this study (glass/ITO/P3HT:PCBM/Al).

In order to perform the present investigation, the EDXR set-up was modified in order to allow a direct comparison of the structural changes with the working efficiency of the device (see experimental section). This new set-up permits simultaneous monitoring of the PV cell photo-current and the morphological changes (by EDXR) in order to correlate the oxidation process with the decline of the device performances.

In the present paper, we also discuss the effect of a preventive annealing process on cell morphology and efficiency.

Since the device is a multilayered system, as shown in Fig. 1, in order to identify the contributions of each layer to the overall X-ray reflection signal, EDXR measurements on samples that correspond to the subsequent stages of cell construction were performed. The reflection patterns of samples that correspond to such stages were compared with the patterns of the complete cell shown in Fig. 2. In particular, for the measurements of the cells, an experimental procedure was used to maximize the Al signal with respect to the one coming from the other layers, in particular from indium thin oxide (ITO). It consisted of tilting slightly the sample under the X-ray beam, by means of a rotating cradle. In this way, it was possible to assign the oscillations visible at lower scattering vectors (curve b in Fig. 2) to the Al film, the period of the oscillations being related to the film thickness d [16]. These preliminary measurements also allowed the determination of the total reflection edge with higher accuracy, in comparison with previous works [12,13].

At higher scattering vectors, the effect of the presence of the other layers is more evident, and an interference pattern in the thickness fringes is visible. For this reason, the fit in Fig. 2 is limited to the lower scattering vector region, where the Al contribution is dominant.

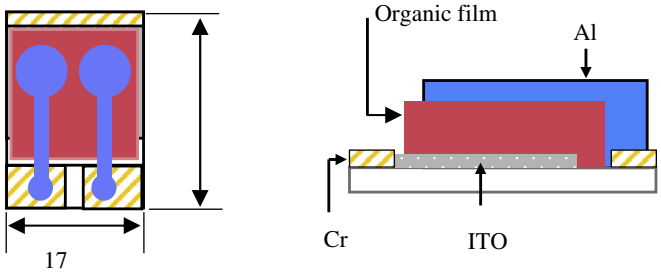

Fig. 1. Sketch of the device is shown.

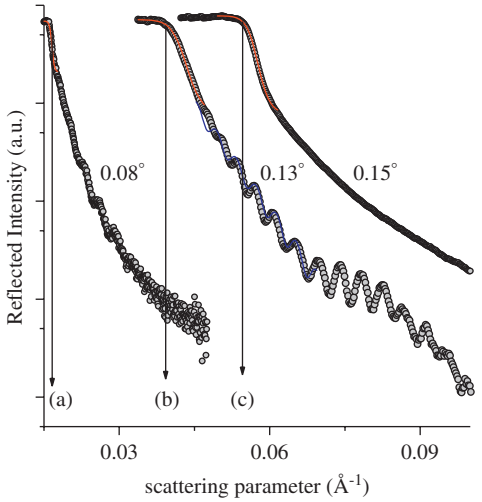

Fig. 2. The reflection patterns of samples corresponding to the various stages of the cell construction are compared with the patterns of the complete cell. The scattering length densities ρ_e of the various layers are: (a) glass/ITO/P3HT:PCBM, $\rho_e = 9.6(1) \times 10^{-6}$ Å^{-2}; (b) glass/ITO/P3HT:PCBM/Al, $\rho_e = 2.9(1) \times 10^{-5}$ Å^{-2}; (c) glass/ITO, $\rho_e = 5.6(1) \times 10^{-5}$ Å^{-2}.

Conversely, no Kiessig fringes are visible in curve c (glass/ITO sample), probably due to its severe roughness. Indeed, the rather low resolution of the solid-state detector used in the ED mode rounds the cuspids in the reflection patterns, but does not change the oscillation frequency. Therefore, for films whose thickness d ranges from tenths to hundreds of nanometers, the changes of d as a function of time can be accurately determined. Above such high thickness limit, the poor energy resolution of the detector makes it difficult to resolve the Kiessig fringes, especially when the sample is rough (as in the case of the ITO layer).

Of particular interest is the fact that the derivative of the reflection profile fit provides an accurate determination of the total reflection edges of the X-ray reflectivity patterns, and as a result the scattering length densities of the various layers can be obtained. These values can be compared with those calculated theoretically on the basis of the nominal densities of the materials, and this information can be used to impose some constraint on the parameter in the Parratt formula [17] utilized to fit the reflection patterns. The formula, usually utilized to fit reflection data collected in the AD mode, has been adapted to the ED case [11].

The result is the following:

$$|R|^2 = \{1 - 2[(\mathrm{Real}(R_l^* R_r - R_l R_r)\exp(-2kd)]/[1 + \exp(-4kd) - 2\mathrm{Real}(R_l R_r)\exp(-2kd)]\},$$

where $R_l = (k_0 - k)/(k_0 + k)$ is the Fresnel film reflectivity, $R_r = (k - k_s)/(k + k_s)$ is the Fresnel substrate reflectivity, $k_0 = q/2$ is the radiation wave number in air and d is the film average thickness.

The quantities k and k_s are the radiation wave numbers in the film and in the substrate, respectively, which depend on k_0:

$$k_f = (k_0^2 - 4\pi\rho)^{1/2} \text{ and } k_s = (k_0^2 - 4\pi\rho_s)^{1/2}.$$

When the surface or interface is not sharp, the reflected intensity is modified by introducing a convenient roughness parameter, generally the Nevot–Croce factor. Considering only the dominant term of the film surface roughness, the general expression for the reflected intensity is

$$|R|^2 = \{|R_l|^2 \exp(-2kk_0\sigma^2)| + ||R_r|^2 - 2\mathrm{Re}[R_l R_r \exp(-2kk_0\sigma^2)\exp(2ikd)]/1 + |R_l|^2|R_r|^2 \exp(-2kk_0\sigma^2)| - 2\mathrm{Re}[R_l R_r \exp(-2kk_0\sigma^2)\exp(2ikd)]\}.$$

Therefore, five free parameters are normally used in the fit, one to normalize the intensities to the counting times, the others giving the morphological parameters of interest: the substrate scattering length density, the film scattering length density, the average thickness of the film and its surface roughness, defined analytically as the standard deviation from the (average) thickness. The same model was applied in the present study, limiting the fit to the lower scattering vector region, where the Al contribution is dominant.

The results of the in situ EDXR measurements, collected under a controlled N_2 atmosphere and upon illumination with a white light lamp, are shown in Fig. 3.

The reflectivity profiles do not show any changes in the oscillation period when the sample is kept in the dark (first patterns on the bottom of the graph which are shifted in height for clarity). However, a progressive compression of the Kiessig fringes, during illumination, can be noticed corresponding to an increase of the Al film thickness, as a direct consequence of exposure to light. Such an ageing effect may be attributed to the formation of an aluminium oxide layer at the Al/organic film interface [12], as a

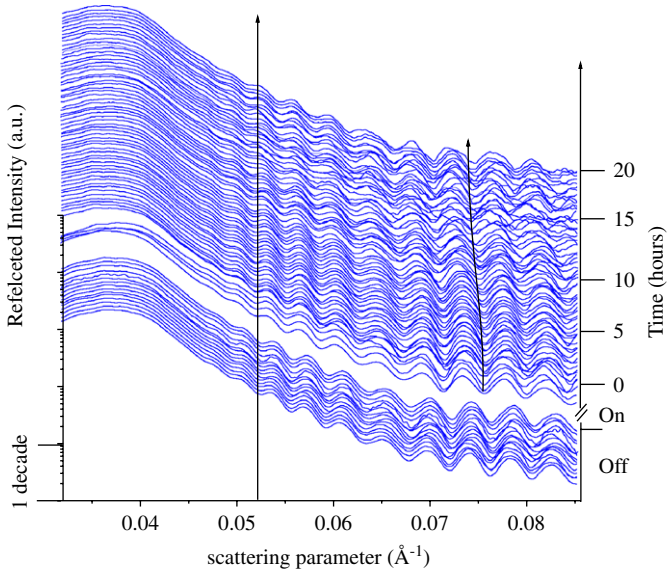

Fig. 3. EDXR in situ measurements, collected under controlled atmosphere and upon illumination on the pristine PV cell. The transient modification of the reflectivity plateau visible along the first three patterns after lightening is due to the refill of liquid nitrogen in the solid-state detector cryostat.

consequence of illumination. Indeed, the aluminium layer in the device is in contact with the oxygen ions (bounded to the polymers of the organic layer), which may be released during illumination, so that photo-induced oxidation may well occur. Moreover, samples have been stored in the dark under ambient conditions before being measured, and a certain amount of humidity may have been absorbed by the organic layer.

The aluminium oxidation process appears as a thickening of the Al film, because it leads to the formation of a thin layer of aluminium oxides, too thin to be detected by the EDXR technique as a separate layer. Moreover, the interface between the aluminium oxide and the polymer is likely not sharp. As a consequence, in the reflection interaction, it is felt by the X-rays as an increase of the Al bulk, rather than as an independent, well-defined layer.

In the following, we will discuss how the time-resolved EDXR measurements validate this hypothesis.

The resulting d vs. time data points, obtained by the fit of the patterns in Fig. 3, are plotted in Fig. 4b. The stability of the morphology in the dark was verified for a long period. The subsequent effect of illumination is visibly a two-step increase in thickness. The fit of the $d(t)$ curves was carried out using two correlated Boltzmann curves: the first curve, $d(t) = d_1 + (d_2 - d_1)\ (1 - \exp(t/\tau_1))$, describes the progressive increase of the film thickness d from its initial value d_1 up to a first asymptotical value d_2 in a characteristic time τ_1; the second one, $d(t) = d_3 + (d_4 - d_3)\ (1 - \exp(t/\tau_1))$, describes a further increase in thickness, beginning when the film thickness has reached the intermediate value d_3 until a final asymptotical value d_4 in a characteristic time τ_2. It can be noticed that the first process is almost concluded at the onset of the second. This characteristic provides further qualitative information that clarifies the nature of such processes, and supports the hypothesis that electrode oxidation has taken place. Indeed, the Al oxidation kinetics is expected to be a two-step process, where the formation of suboxides is the precursor to the growth of a passivating layer of alumina [18].

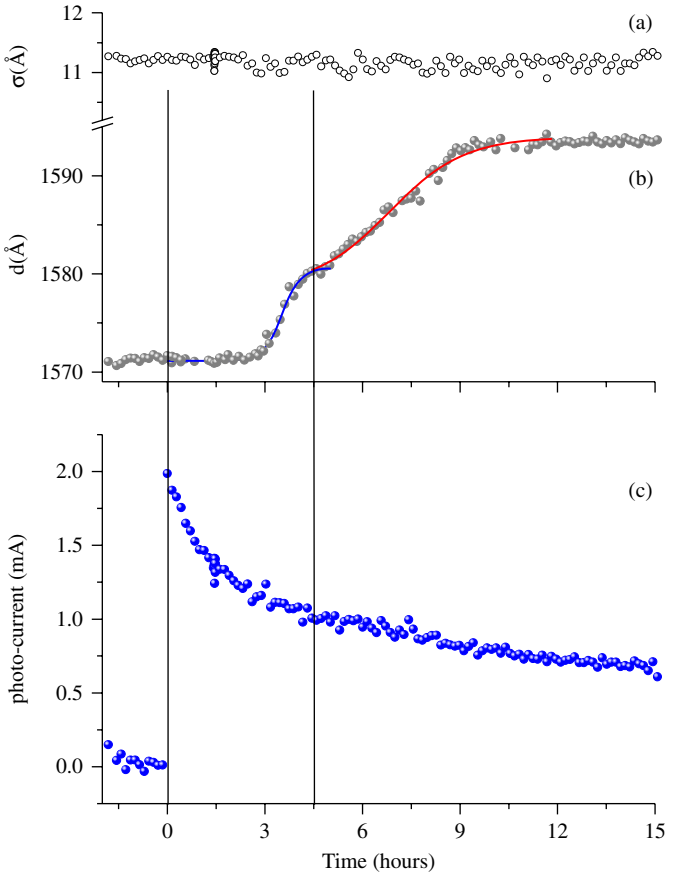

Fig. 4. Results of data fit (film roughness σ vs. time, film thickness d vs. time) and cell photo-current measured during the EDXR experiment.

The σ vs. t data points plotted in Fig. 4a show that this parameter remains unchanged during the overall process. Since surface phenomena normally produce an increase of the film surface roughness, the fact that in the present case no modification of this parameter is observed over time is a substantial clue that the process is limited to the interface between the aluminium and the organic film, no variation of the surface being expected.

During the EDXR measurements, the cell photo-current was monitored and the result is reported in Fig. 4c. It allows the photo-oxidation process of the electrode (observed by EDXR) to be directly correlated with the fading of the cell performances. Moreover, it is worth noticing how the time evolution of the morphological data, due to the elevated temporal sampling, is able to describe the dynamics of this process. Indeed, it is understood that the process takes place in two steps (see Fig. 4b), while the electrical measurements, normally used to define the ageing effects in PV devices (see Fig. 4c), are unable to provide this information.

Another important result that was obtained is the direct evidence that such photo-induced degradation processes at the electrode–heterojunction interface can be inhibited by submitting the sample to a preventive annealing procedure. This can be deduced by observing the data in Fig. 5, which represents EDXR patterns recorded *in situ* on illumination for a PV device analogous to the former, but that had previously been annealed at 100 °C for 30 min. The patterns are perfectly overlapping, demonstrating that no photo-induced oxidation of the Al–organic film is present.

In turn, such morphological stability assures improved contact between the active layer and the metal electrode, increasing the efficiency of the annealed cell by almost an order of magnitude.

This is evident when comparing the J/V characteristics under simulated AM1.5 100 mW/cm^2 illuminations of two cells, one of which had been submitted to prior annealing at 100 °C for 30 min (see Fig. 6). The PV parameters are: $V_{oc} = 0.454$ V, $J_{sc} = 2.0$ mA/cm^2, FF = 0.35%, $\eta = 0.3\%$ for the pristine cell and $V_{oc} = 0.604$ V, $J_{sc} = 7.5$ mA/cm^2, FF = 0.57% and $\eta = 2.6\%$ for the annealed cell.

Although a full interpretation of the origin of the morphological stabilizing effect induced by the annealing procedure needs further investigation, its positive effect on

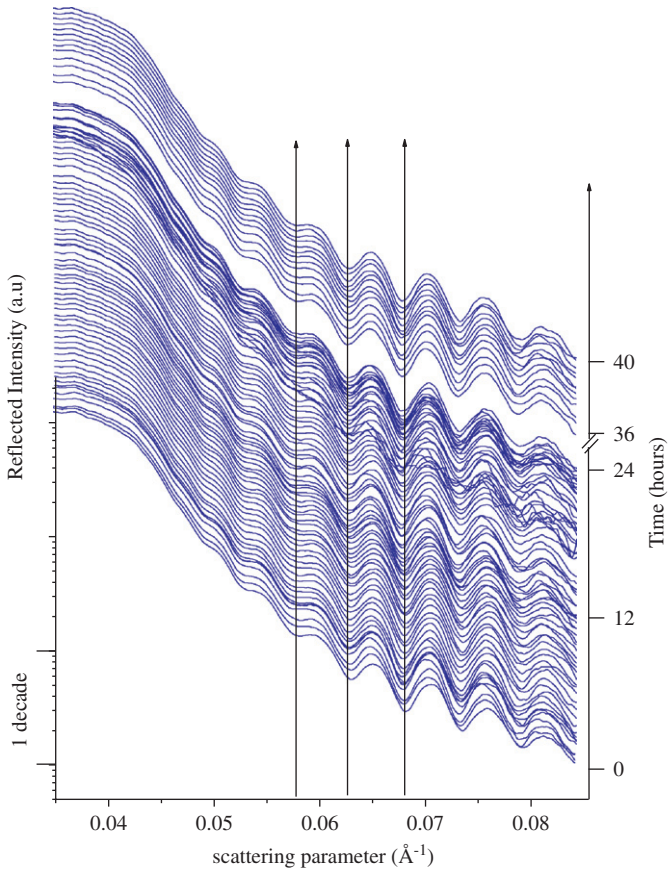

Fig. 5. EDXR in situ measurements, collected under controlled atmosphere and upon illumination on the annealed PV cell.

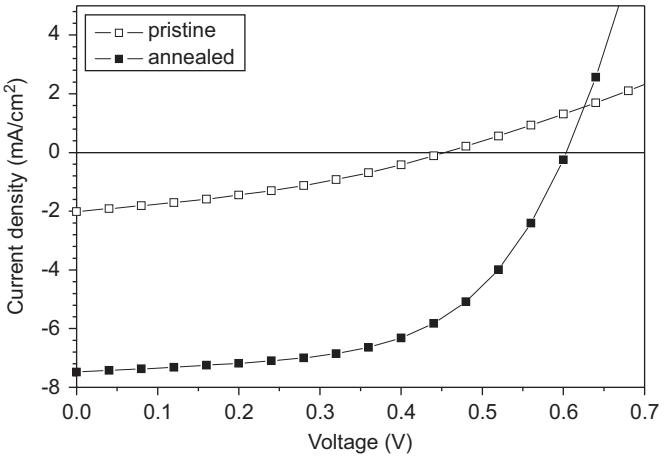

Fig. 6. The J/V characteristics under simulated AM1.5, 100 mW/cm^2 illumination conditions are shown for both the pristine and the annealed cells.

the device efficiency can be considered as an acquired result.

3. Conclusions

In conclusion, we report the first in situ study correlating the variation of the photo-current of the device upon working to the electrode–organic film interface morphological evolution monitored by the time-resolved EDXR technique.

The study demonstrated a direct connection between the real time morphological changes and the decline in performance of the working device. This experimental approach gave several important results.

First, the morphological changes in the device structure (undergoing a photo-induced oxidation of the Al–organic film interface) strongly affect the response of the system.

Second, the comparison of the electrical and EDXR data sets shows that, while the photo-current vs. time curve reveals only the occurrence of a photo-degradation phenomenon, the in situ EDXR technique is able additionally to describe the dynamics of this effect. In particular, the observed process is limited to the buried electrode interface, and is responsible for a rapid decrease in the photo-current.

Finally, it was shown that the interface morphology may be stabilized by annealing treatments, resulting in a significant improvement of cell efficiency.

The results indicate that the proposed method, making simultaneous use of morphological and electrical monitoring techniques, can be successfully used to investigate new organic devices in real operating conditions, therefore deepening our knowledge of all the phenomena that influence their performances.

4. Experimental

4.1. Sample preparation

The bulk heterojunction solar cells used in this article were made from a blend of methano-fullerene [6,6]-phenyl C_{61} butyric acid methyl ester, denoted as PCBM, and P3HT. The cells consisted of an ITO substrate cleaned in an ultrasonic bath of acetone and isopropanol, rinsed in deionized water, dried in an oven and, finally, treated with UV-ozone. The active layer of P3HT:PCBM was deposited by spin casting from an anhydrous chlorobenzene solution, and the devices were completed by deposition of the cathode through a shadow mask with 6 mm diameter openings. The top contact was a 100-nm-thick Al layer (nominal thickness). The cells had an active surface of 32 mm^2. The annealing was performed in a glove box under controlled atmosphere (<1 ppm O_2 and H_2O).

4.2. X-ray and photo-current set-up

The experimental apparatus consisted of a non-commercial reflectometer [11] characterized by a very simple set-up geometry, since neither monochromator nor goniometer is required in the ED mode, no movement being needed during the measurements. The main elements of the machine are an X-ray tube and an energy-sensitive detector, mounted on two benches pivoting around a common central axis. Four adjustable slits are used to

define the X-ray optical path. The Bremmsstrahlung of the X-ray tube (3 kW power, tungsten anode) is used as a probe, and an EG&G high-purity germanium solid-state detector, whose energy resolution is about 1.5–2% in the 15–50 keV energy range, accomplishes the energy scan. The measurements were performed with the device placed inside an X-ray transparent chamber, under an N_2 gas flux. Sample alignment was checked during the experiment to detect and keep under control possible misalignments of the sample due to heating during illumination.. During the EDXR measurements, the photo-current was monitored by using a home-made acquisition software running over Labview. Measurements were carried out in short circuit conditions during illumination with a white light lamp ($10\,mW/cm^2$).

Acknowledgements

The authors are grateful to Dr. A. Casling and Dr. D.-T. Ton-That for their critical reading of the manuscript.

References

[1] N.S. Sariciftci, L. Smilowitz, A.J. Heeger, F. Wudl, Science 258 (1992) 1474.
[2] C.J. Brabec, Sol. Energy Mater. Sol. Cells 83 (2004) 273.
[3] X.N. Yang, J. Loos, S.C. Veenstra, W.J.H. Verhees, M.M. Wienk, J.M. Kroon, M.A.J. Michels, R.A.J. Janssen, Nano Lett. 5 (4) (2005) 579.
[4] F.C. Krebs, H. Spanggaard, Chem. Mater. 17 (21) (2005) 5235.
[5] R. de Bettignies, J. Leroy, M. Firon, C. Sentein, Synth. Methods 156 (2006) 510.
[6] G. Li, V. Shrotriya, J.S. Huang, Y. Yao, T. Moriarty, K. Emery, Y. Yang, Nat. Mater. 4 (11) (2005) 864.
[7] Y. Kim, S. Cook, S.M. Tuladhar, S.A. Choulis, J. Nelson, J.R. Durrant, D.D.C. Bradley, M. Giles, I. Mcculloch, C.S. Ha, M. Ree, Nat. Mater. 5 (3) (2006) 197.
[8] J. Peet, J.Y. Kim, N.E. Coates, W.L. Ma, D. Moses, A.J. Heeger, G.C. Bazan, Nat. Mater. 15 (10) (2007) 1617.
[9] K. Kim, J. Liu, M.A.G. Namboothiry, D.L. Caroll, Appl. Phys. Lett. 90 (2007) 163511.
[10] W. Ma, C. Yang, X. Gong, K. Lee, A.J. Heeger, Adv. Funct. Mater. 15 (10) (2005) 1617.
[11] V. Rossi Albertini, B. Paci, A. Generosi, J. Phys. D: Appl. Phys. 39 (2006) 461.
[12] B. Paci, A. Generosi, V. Rossi Albertini, P. Perfetti, R. de Bettignies, M. Firon, J. Leroy, C. Sentein, Appl. Phys. Lett. 87 (2005) 194110.
[13] B. Paci, A. Generosi, V. Rossi Albertini, P. Perfetti, R. de Bettignies, M. Firon, J. Leroy, C. Sentein, Appl. Phys. Lett. 89 (2006) 043507.
[14] R.W. James, The Optical Principles of the Diffraction of X-ray, OX BOW Press, Woodbridge, CT, 1982.
[15] R. Caminiti, V. Rossi Albertini, Int. Rev. Phys. Chem. 18 (2) (1999) 263.
[16] S.K. Sinha, E.B. Sirota, S. Garoff, H.B. Stanley, Phys. Rev. B 38 (1988) 2297.
[17] L.G. Parrat, Phys. Rev. 95 (1954) 359.
[18] G. Faraci, S. La Rosa, A.R. Pennisi, Y. Hwu, G. Margaritondo, Phys. Rev. B 47 (1993) 4052.